*J. Fluid Mech.* (1978), *vol.* 87, *part* 1, *pp.* 97–120
*Printed in Great Britain*



# Flow in the entrance of the aorta

By M. P. SINGH, P. C. SINHA
AND MEENA AGGARWAL
Department of Mathematics, Indian Institute of Technology, New Delhi

(Received 28 February 1977)

This paper supplements an earlier study (Singh 1974) of the steady case of 'Entry flow in a curved pipe'. Here we consider an entrance profile of the form

$$w = Q(t)/(1 + \delta r \cos\alpha),$$

which is physiologically more relevant for blood being pumped from the left ventricle into the ascending aorta. A boundary-layer analysis is applied to determine the effects of curvature and an adverse pressure gradient (associated with the primary flow) on the wall shear. The study shows how the negative wall shear and backflow near the wall develop during the decelerating phase of the cycle as the boundary layer grows. The analysis shows how the increasing effect of the secondary flow due to curvature draws off slower moving fluid azimuthally from the outer bend to the inner bend; this induces a cross-flow of faster moving fluid from the inner bend to the outer bend which results in a thinning of the boundary layer at the outer bend and a thickening at the inner bend. This implies an increased wall shear at the outer bend compared with that at the inner bend as the flow develops further downstream; this is in contrast with the initial stages of the motion near the entrance where the higher wall shear occurs at the inner bend owing to the external flow and to geometric factors. The analysis shows that the displacement effect of the boundary layer on the core is not significant because the boundary layer remains thin, about one-tenth of the tube diameter.

## 1. Introduction

A study of the oscillatory flow of viscous fluid in a curved tube is a step towards the simulation of blood flow at curvature sites. For such flows an understanding of the distributions of velocities, shear stresses and pressure may help to provide some understanding of the genesis of certain arterial diseases. Curvature sites have been associated with the onset of atherosclerosis (Wolstraholme & Knight 1973), which is one of the principal causes of circulatory failure. Lesions are distributed non-uniformly around the surface of arteries, being more commonly found near bifurcations, on the inner walls of curves, and in larger arteries. The regions where lesions tend to develop are closely correlated both with areas of the wall in which the endothelial cells are found experimentally to have a relatively low permeability to large molecules such as lipoproteins, which are known to be implicated in the generation of the lesions, and with areas which would be expected to experience a relatively low wall shear (see Lighthill 1975). Detailed patterns of wall stress associated with blood flow may play a causative role in atherogenesis. The secondary flows induced by the centrifugal

effects developed at curvature sites will result in asymmetrical wall stresses with a high-shear region and a low-pressure region. Texon postulates a suction effect in the low-pressure region as a cause for the onset of incipient atheroma (Chandran *et al.* 1974). Fry has demonstrated that extremely high shearing stresses are able to produce actual mechanical damage to the endothelial lining of the arterial wall which can foster the development of atherogenesis. On the other hand Caro, Fitz-Gerald & Schroter (1971) consider that the fluid mechanics of blood flow has a controlling and inhibiting effect, rather than a causative one, in atherogenesis. They correlate the observed natural cases of incipient atheroma with a low-shear region and suggest a shear-dependent mass-transfer mechanism in explaining this phenomena. It is likely that all the above-mentioned factors (including exceptionally high or exceptionally low stress) may be contributory. In any case, it is essential to know the distributions of velocity, pressure and shear stresses so that correlations with further controlled experiments could help in providing more definitive explanations for this common fatal disease of modern society.

This paper studies the problem with particular reference to the ascending aorta. This is an elastic tube that stems from the left ventricle of the heart, curving in a complicated three-dimensional way and giving off branches to the head and upper limbs. The heart generates a periodic pressure gradient which is transmitted as a travelling wave whose velocity is an order of magnitude greater than the fluid velocity. In our analysis, the ascending aorta is modelled as a uniform, curved and rigid tube. We ignore the fact that the aorta is twisted and although the branches from the arch of the aorta will clearly have a significant influence on the flow near their entrances, their effect on the flow nearer to the heart is likely to be less pronounced (Nerem, Seed & Wood 1972). We also ignore the wall distensibility, which is important in determining how the pulse wave propagates, which in turn determines the local pressure gradient [proportional to $\dot{Q}$; see (1)] as a function of time. However, the flow response to that gradient is approximately the same as in a rigid tube, both because the wave length is large compared with the length of the ascending aorta, and because the wave speed is large compared with the fluid speed. (The typical variations of arterial diameter as a pulse passes are only about $\pm 2\,\%$ and the pulse wave velocity is at least five times the maximum blood velocity, so that neglecting arterial wall elasticity and thereby making the effect of pressure changes propagate infinitely fast would not entail significant errors in the analysis (Lighthill 1975). A similar argument shows that the taper of the aorta is also unimportant.)

The two factors that now distinguish the problem from that of a classical entrance length are the curvature of the tube, and the fluctuations in the flow rate. We assume blood to be incompressible, homogeneous in composition and rheologically Newtonian with a constant viscosity. In the applications to blood flow, we are, therefore, assuming that the non-Newtonian and non-homogeneous properties of blood (which, after all, is a concentrated suspension of flexible red cells) can be ignored. This is justified so long as the shear rates in the fluid do not fall below $100\mathrm{S}^{-1}$, and so long as the length scales of the flow are large compared with the cell diameter and spacing, which are of the order of $10\,\mu$m (Whitmore 1968, chap. 6). The flow is considered laminar, although non-laminar disturbed flows have been observed in larger arteries where highly pulsatile flows with relatively high peak velocities occur. For instance, McDonald (1952) reports that, in the rabbit aorta, the laminar flow which exists over the great

portion of the pulse cycle breaks down and becomes turbulent over a portion of the pulse cycle about 50 milliseconds in duration, when the velocity is at its peak (see also Seed & Wood 1971; Nerem & Seed 1972; Hall & Parker 1976). The temporal and spatial behaviour of the fluid velocity and pressure is assumed to be known at the tube entrance and is taken to be periodic in time. For the aorta the flow is injected periodically through the aortic valve by the contraction of the left ventricle, and it might be expected that the entrance flow is somewhat jet-like and hence rather uniform across the vessel, although some radial and azimuthal dependence is probably also present (see Bellhouse & Talbot 1969). It is further assumed that no backflow occurs as the aortic valve closes. Physiologically, however, backflow occurs over a small portion of the pulse cycle as the diastolic phase starts, presumably because of arterial wall distensibility (McDonald 1960; Nerem *et al.* 1972; Pedley 1976; see also figure 2). Finally, we neglect all external body forces and the system is assumed to be undergoing a general, steady-state periodic motion of constant period (of course, time-independent components may also be present), no transients being involved.

Although the mathematical model neglects certain physical effects which exist in the vascular system, it still retains the important characteristics of the blood flow near the aortic valve, the neglected effects being of secondary importance. It might also be mentioned that although the motivation for this study has come from physiological considerations, the model could also conceivably be applied to other situations, such as fluidic devices, hydraulic control lines, etc.

Several studies have recently considered entrance effects on the fluid motion in a curved pipe (see, for example, Olson 1971 for an experimental study; Patankar, Pratap & Spalding 1974 for a numerical study; Singh 1974 and Yao & Berger 1975 for analytical studies). However, all of these studies are confined to steady-state situations. Here we extend Singh's (1974) analysis to the physiologically interesting case of pulsatile entry flow and discuss the effects of curvature and adverse pressure gradient (associated with the primary flow) on the wall shear. The analysis shows how the negative wall shear and backflow near the wall develop during the decelerating phase of the cycle as the boundary layer grows. The study shows how the increasing effect of the secondary flow due to the curvature draws off slower moving fluid azimuthally from the outer bend to the inner and induces a cross-flow of faster moving fluid from the inner bend to the outer which results in a thinning of the boundary layer at the outer bend and a thickening at the inner bend. This implies a higher wall shear at the outer bend in comparison with that at the inner bend as the flow develops further downstream. This is in contrast to the initial stages of the motion near the entrance, where the higher wall shear occurs at the inner bend because of the external flow and geometric factors. The analysis shows that the displacement effect of the boundary layer on the core is not significant because the boundary layer remains thin.

## 2. Formulation of the problem

Figure 1 shows the system of toroidal co-ordinates $(r', \alpha, \theta)$ with which we study the motion of fluid through a pipe which has a circular cross-section and which is coiled in the form of a circle. The axis of the circle into which the pipe is coiled is $OZ$ and $C$ is the centre of the cross-section of the pipe in a plane that makes an angle $\theta$ with the fixed axial plane. $OC$ is of length $L$, which is the radius of curvature of the

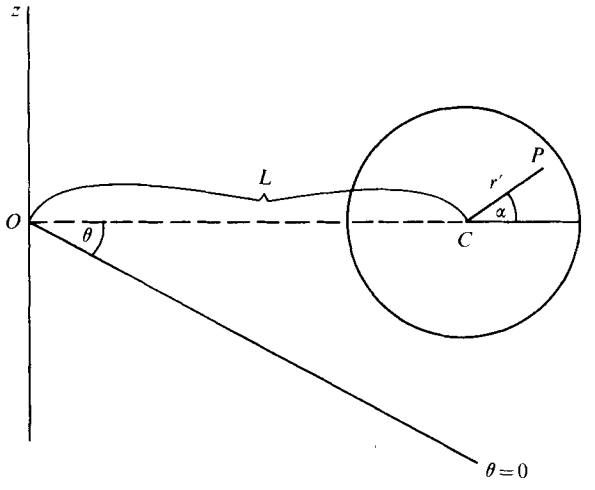


FIGURE 1. Geometrical configuration of the problem in toroidal co-ordinates $(r', \alpha, \theta)$.

coiled tube. The plane passing through $O$ and perpendicular to $OZ$ will be called the 'central plane' of the pipe and the circle traced out by $C$ the pipe's 'central line', $r'$ denotes the distance $CP$ and $\alpha$ is the angle which $CP$ makes with the line $OC$ produced. Let $(u', v', w')$ denote the corresponding velocity components in the $(r', \alpha, \theta)$ directions at time $t'$.

*Entry and boundary conditions*

No precise data are available for the blood velocity at the aortic entrance. We assume here that the dynamic pressure across the cross-section at the entrance to the bend is constant, which corresponds to the curved pipe taking the fluid from a reservoir at constant pressure. In this case, the injection velocity is given by

$$u' = v' = 0, \quad w' = L\overline{W}_0 Q(\omega t')/(L + r' \cos\alpha). \tag{1}$$

Since the backflow at the entrance is not considered, we impose the important restriction

$$Q \geqslant 0. \tag{2}$$

Although the analysis is developed for general $Q$ satisfying (2), detailed calculations are done for the following cases:

$$Q = 1 + 0{\cdot}8 \sin t \quad \text{for} \quad 0 \leqslant t \leqslant 2\pi, \tag{3a}$$

and

$$Q = \begin{cases} (1 - \cos \frac{8}{3}t)^3 & \text{for} \quad 0 \leqslant t \leqslant \frac{3}{4}\pi, \\ 0 & \text{for} \quad \frac{3}{4}\pi \leqslant t \leqslant 2\pi. \end{cases} \tag{3b}$$

The graph of the proposed models of $Q$ may be compared with the typical velocity near the aortic entrance in a dog (McDonald 1960) (see figure 2). The boundary conditions are the usual no-slip and continuity of normal component conditions:

$$u' = v' = w' = 0 \quad \text{at} \quad r' = a. \tag{4}$$

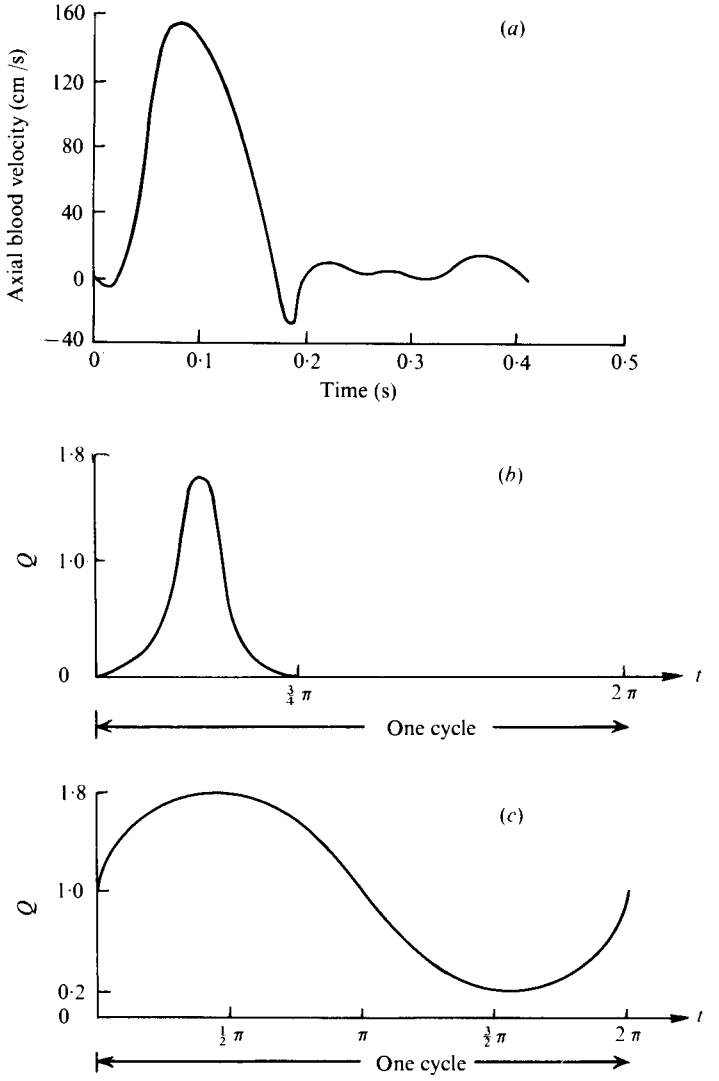


FIGURE 2. (*a*) Typical blood velocity near the aortic entrance in a dog. (Note that this velocity is an average over the cross-section of the artery and is proportional to the instantaneous volume flux.) From McDonald (1960). (*b*), (*c*) Entrance profiles for which computations have been carried out: (*b*) profile (3*a*); (*c*) profile (3*b*).

### *Non-dimensional equations of motion*

Near the entrance, it is natural to refer the velocity to the characteristic entrance velocity $\overline{W}_0$, the co-ordinates $r'$ and $s' = L\theta$ to $a$, the pressure to $\rho\overline{W}_0^2$ and time to $1/\omega$, where $\rho$ is the density of the fluid. The following physiological data will be taken into account for estimating the orders of magnitude of the parameters arising in the dimensionless equations of motion: radius $a$ of the ascending aorta = 1·15 – 2·18 cm (for man) or 0·50 cm (for dogs; see McDonald 1960); kinematic viscosity of blood $\nu$ = 0·038 cgs units at 37 °C (for man); the duration of each systole (for man) is approximately 0·3 s, during which about 80 ml of blood is pumped from the left ventricle into the ascending aorta. The frequency of the systolic cycle is approximately 70 $\text{min}^{-1}$;

$\omega$ is $2\pi$ times this frequency. Accordingly, the curvature ratio $\delta = a/L = O(10^{-1})$, the Reynolds number $Re = a\overline{W}_0/\nu = O(10^3)$, and the frequency parameter

$$\epsilon = a\omega/\overline{W}_0 = O(10^{-1}).$$

The equations of motion are

$$u_r + (1 + 2r\delta\cos\alpha)\,u/rR(r,\alpha) + v_\alpha/r - v\delta\sin\alpha/R(r,\alpha) + w_s/R(r,\alpha) = 0, \tag{5}$$

$$\begin{aligned}\epsilon u_t + uu_r + vu_\alpha/r + wu_s/R(r,\alpha) - v^2/r - w^2\delta\cos\alpha/R(r,\alpha)\\ = -p_r - (Re)^{-1}[(r^{-1}\partial/\partial\alpha - \delta\sin\alpha R^{-1})(v_r + v/r - u_\alpha/r) - u_{ss}/R^2(r,\alpha)\\ + w_{rs}/R(r,\alpha) + w_s\delta\cos\alpha/R^2(r,\alpha)],\end{aligned} \tag{6}$$

$$\begin{aligned}\epsilon v_t + uv_r + vv_\alpha/r + wv_s/R(r,\alpha) + uv/r + w^2\delta\sin\alpha/R(r,\alpha)\\ = -p_\alpha/r + (Re)^{-1}[v_{ss}/R^2(r,\alpha) - w_{s\alpha}/rR(r,\alpha)\\ + w_s\delta\sin\alpha/R^2(r,\alpha) + (\partial/\partial r + \delta\cos\alpha/R(r,\alpha))(v_r + v/r - u_\alpha/r)],\end{aligned} \tag{7}$$

$$\begin{aligned}\epsilon w_t + uw_r + vw_\alpha/r + ww_s/R(r,\alpha) + uw\delta\cos\alpha/R(r,\alpha) - vw\delta\sin\alpha/R(r,\alpha)\\ = -p_s/R(r,\alpha) + (Re)^{-1}[(\partial/\partial r + r^{-1})(w_r + w\delta\cos\alpha/R - u_s/R)\\ + w_{\alpha\alpha}/r^2 - r^{-1}\partial(v_sR^{-1})/\partial\alpha - r^{-1}\partial(w\delta\sin\alpha R^{-1})/\partial\alpha],\end{aligned} \tag{8}$$

where the unprimed variables are in dimensionless form, the parameters $\epsilon$, $\delta$ and $Re$ are defined above, and $R(r,\alpha) = 1 + r\delta\cos\alpha$.

The corresponding entry and boundary conditions in the non-dimensional form become

$$u = v = 0, \quad w = Q(t)/R(r,\alpha) \quad \text{at} \quad s = 0, \tag{9a}$$

and

$$u = v = w = 0 \quad \text{at} \quad r = 1. \tag{9b}$$

It may be noted that, in the absence of viscosity, the exact solution of the above equations satisfying the entry conditions (9*a*) is

$$u = v = 0, \quad w = Q(t)/R(r,\alpha), \quad p = -\tfrac{1}{2}Q^2/R^2(r,\alpha) - \epsilon s\dot{Q}, \tag{10}$$

where $\dot{Q} = dQ/dt$.

## 3. Solution

Since the Reynolds number $Re$ is $O(10^3)$, Singh's (1974) analysis for the steady entry problem is applicable here. As the fluid is injected into the pipe, the central core of the fluid will not be influenced by viscosity, whose effects will be confined to a thin layer near the wall of the tube. Therefore, the flow can be divided into two regions: (i) an inviscid core in which the centrifugal force due to the curved motion of the main body of the fluid along the tube is balanced by the pressure gradient directed towards the centre of curvature and in which the instantaneous axial fluid acceleration is sustained by the streamwise pressure gradient, and (ii) a thin boundary layer in which the viscous forces are balanced by the inertia forces. As in the classical boundary layer, pressure will be transmitted to the flow in the boundary layer by the external flow, which implies that the azimuthal pressure gradient, which is of second order during the initial stages of motion, will induce a transverse flow in the boundary layer from the outside of the bend towards the inside. The effect of the growing boundary layer on the flow in the core will be to accelerate the motion due to the displacement

effect of the boundary layer, and the effect of the second-order transverse flow in the boundary layer will be to induce a cross-flow from the inside of the bend towards the outside to satisfy the mass conservation principle. The secondary flow due to the curvature effects in the region close to the entry can, therefore, be obtained by perturbing the solution for developing flow in a straight tube.

*First-order solution in the inviscid core*

The solution in the core is just the undisturbed entry flow

$$u = v = 0, \quad w = Q(t)/R(r,\alpha), \quad p = -\tfrac{1}{2}Q^2/R^2 - \epsilon s\dot{Q} + f(t), \tag{11}$$

where $f(t)$ is the left ventricular pressure (determined by the total impedance of the cardiovascular system), and $R = 1 + r\delta\cos\alpha$ as before.

*First-order boundary layer*

As in the flat-plate case (Pedley 1976), there will be an approximately quasi-steady boundary layer in which the convective inertia forces are balanced by the viscous forces and the unsteady inertia terms are first-order small quantities. Accordingly, we introduce

$$r = 1 - \beta\eta, \quad u = \beta Q\tilde{u}, \quad v = Q\tilde{v}, \quad w = Q\tilde{w}, \quad p = Q^2\tilde{p}, \tag{12}$$

where $\beta^2 = \nu/a\overline{W}_0 Q$ and $\beta^{-2}$ equals the instantaneous Reynolds number of the flow.

Substituting these magnified variables into (5)–(8) and retaining the leading terms, we obtain

$$-\tilde{u}_\eta + \tilde{v}_\alpha - \tilde{v}\delta\sin\alpha/R(1,\alpha) + \tilde{w}_s/R(1,\alpha) = 0, \tag{13a}$$

$$\tilde{p}_\eta = 0, \tag{13b}$$

$$\epsilon\left[\frac{\dot{Q}}{Q^2}\tilde{v} + \frac{\tilde{v}_t}{Q} + \frac{\eta\dot{Q}}{2Q^2}\tilde{v}_\eta\right] - \tilde{u}\tilde{v}_\eta + \tilde{v}\tilde{v}_\alpha + \tilde{w}\tilde{v}_s/R(1,\alpha) + \tilde{w}^2\delta\sin\alpha/R(1,\alpha) = -\tilde{p}_\alpha + \tilde{v}_{\eta\eta}, \tag{13c}$$

$$\epsilon\left[\frac{\dot{Q}}{Q^2}\tilde{w} + \frac{\tilde{w}_t}{Q} + \frac{\eta\dot{Q}}{2Q^2}\tilde{w}_\eta\right] - \tilde{u}\tilde{w}_\eta + \tilde{v}\tilde{w}_\alpha - \tilde{v}\tilde{w}\delta\sin\alpha/R(1,\alpha) + \tilde{w}\tilde{w}_s/R(1,\alpha) = -\tilde{p}_s/R(1,\alpha) + \tilde{w}_{\eta\eta}. \tag{13d}$$

The appropriate boundary conditions are

$$\tilde{u} = \tilde{v} = \tilde{w} = 0 \quad \text{at} \quad \eta = 0, \tag{14a}$$

and the condition of matching with the undisturbed inviscid flow yields

$$\tilde{v} \to 0, \quad \tilde{w} \to 1/R(1,\alpha) \quad \text{as} \quad \eta \to \infty, \tag{14b}$$

which also holds at $s = 0$. In (13) and (14) we have obviously used $R(1,\alpha) = 1 + \delta\cos\alpha$. From (13*b*), it follows that the pressure is impressed on the boundary layer by the external flow and hence

$$\tilde{p} = -\tfrac{1}{2}R^{-2}(1,\alpha) - \epsilon s\dot{Q}/Q^2 + f(t)/Q^2, \tag{15}$$

where the last term does not contribute to the pressure gradient and hence will not be considered further. Since the parameters $\epsilon$ and $\delta$ are $O(\frac{1}{10})$, it would be convenient to expand $\tilde{u}$, etc. in the form

$$\tilde{u}(t,\eta,\alpha,s,\beta,\delta,\epsilon) = \tilde{u}_0(t,\eta,\alpha,s) + \delta\tilde{u}_1(t,\eta,\alpha,s) + \epsilon\tilde{u}_2(t,\eta,\alpha,s) + O(\delta^2,\epsilon\delta,\epsilon^2) + O(\beta), \tag{16}$$

etc.

*$O(1)$ equations, matching and boundary conditions*

Making use of (15) and (16) in (13) and (14) and collecting $O(1)$ terms, we obtain

$$-\tilde{u}_{0\eta}+\tilde{v}_{0\alpha}+\tilde{w}_{0s}=0, \tag{17a}$$

$$-\tilde{u}_0\tilde{v}_{0\eta}+\tilde{v}_0\tilde{v}_{0\alpha}+\tilde{w}_0\tilde{v}_{0s}=\tilde{v}_{0\eta\eta}, \tag{17b}$$

$$-\tilde{u}_0\tilde{w}_{0\eta}+\tilde{v}_0\tilde{w}_{0\alpha}+\tilde{w}_0\tilde{w}_{0s}=\tilde{w}_{0\eta\eta}, \tag{17c}$$

with the corresponding boundary and matching conditions

$$\tilde{u}_0=\tilde{v}_0=\tilde{w}_0=0 \quad \text{at} \quad \eta=0, \tag{18a}$$

$$\tilde{v}_0\to 0, \quad \tilde{w}_0\to 1 \quad \text{as} \quad \eta\to\infty. \tag{18b}$$

It follows that

$$\tilde{v}_0\equiv 0, \tag{19}$$

and $\tilde{u}_0$, $\tilde{w}_0$ satisfy the Blasius equation and so we introduce the similarity variable

$$\zeta=(2s)^{-\frac{1}{2}}\eta, \tag{20}$$

and the stream function $\tilde{\psi}_0$ such that

$$\tilde{u}_0=\tilde{\psi}_{0s}, \quad \tilde{w}_0=\tilde{\psi}_{0\eta}.$$

We now introduce the Blasius function $f_0(\zeta)$ given by $\tilde{\psi}_0=(2s)^{\frac{1}{2}}f_0(\zeta)$, in terms of which

$$\tilde{u}_0=(2s)^{-\frac{1}{2}}[f_0-\zeta f_0'], \quad \tilde{w}_0=f_0', \tag{21}$$

and $f_0$ satisfies the Blasius equation

$$f_0'''+f_0f_0''=0, \quad \text{with} \quad f_0(0)=f_0'(0)=0 \quad \text{and} \quad f_0'(\infty)=1, \tag{22}$$

whose solution is well known.

*$O(\delta)$ equations, matching and boundary conditions*

These are obtained from (13) and (14) by using (15) and (16) and collecting $O(\delta)$ terms:

$$-\tilde{u}_{1\eta}+\tilde{v}_{1\alpha}+\tilde{w}_{1s}-\tilde{w}_{0s}\cos\alpha=0, \tag{23a}$$

$$-\tilde{u}_0\tilde{v}_{1\eta}+\tilde{w}_0\tilde{v}_{1s}+\tilde{w}_0^2\sin\alpha=\sin\alpha+\tilde{v}_{1\eta\eta}, \tag{23b}$$

$$-\tilde{u}_0\tilde{w}_{1\eta}-\tilde{u}_1\tilde{w}_{0\eta}+\tilde{w}_0\tilde{w}_{1s}+\tilde{w}_1\tilde{w}_{0s}-\tilde{w}_0\tilde{w}_{0s}\cos\alpha=\tilde{w}_{1\eta\eta} \tag{23c}$$

with the corresponding boundary and matching conditions

$$\tilde{u}_1=\tilde{v}_1=\tilde{w}_1=0 \quad \text{at} \quad \eta=0, \tag{24a}$$

$$\tilde{v}_1\to 0, \quad \tilde{w}_1\to-\cos\alpha \quad \text{as} \quad \eta\to\infty. \tag{24b}$$

These equations are the same as those whose solution was obtained by Singh (1974). We obtain, therefore, the following result:

$$\tilde{u}_1=(2s)^{-\frac{1}{2}}\cos\alpha[f_1(\zeta)-\zeta f_1'(\zeta)+s^2(2g(\zeta)+5f_2(\zeta)-\zeta f_2'(\zeta))], \tag{25a}$$

$$\tilde{v}_1=sg'(\zeta)\sin\alpha, \tag{25b}$$

$$\tilde{w}_1=\cos\alpha[f_0'(\zeta)+f_1'(\zeta)+s^2f_2'(\zeta)], \tag{25c}$$

where $f_1, f_2$ and $g$ satisfy the system of equations

$$f_1 = -[f_0 + \zeta f_0'], \tag{26a}$$

$$f_2''' + f_0 f_2'' - 4f_0' f_2' + f_0''(2g + 5f_2) = 0, \tag{26b}$$

$$g''' + f_0 g'' - 2f_0' g' = 2(f_0'^2 - 1), \tag{26c}$$

with the boundary conditions

$$f_2(0) = f_2'(0) = 0, \quad f_2'(\infty) = 0, \quad g(0) = g'(0) = 0, \quad g'(\infty) = 0. \tag{27}$$

*$O(\epsilon)$ equations, matching and boundary conditions*

As in the preceding case, the following equations are obtained from (13) by collecting $O(\epsilon)$ terms:

$$-\tilde{u}_{2\eta} + \tilde{v}_{2\alpha} + \tilde{w}_{2s} = 0, \tag{28a}$$

$$-\tilde{u}_0 \tilde{v}_{2\eta} + \tilde{w}_0 \tilde{v}_{2s} = \tilde{v}_{2\eta\eta}, \tag{28b}$$

$$\frac{\dot{Q}}{Q^2}\tilde{w}_0 + \frac{\tilde{w}_{0t}}{Q} + \frac{\eta \dot{Q}}{2Q^2}\tilde{w}_{0\eta} - \tilde{u}_0 \tilde{w}_{2\eta} - \tilde{u}_2 \tilde{w}_{0\eta} + \tilde{w}_0 \tilde{w}_{2s} + \tilde{w}_2 \tilde{w}_{0s} = \frac{\dot{Q}}{Q^2} + \tilde{w}_{2\eta\eta}, \tag{28c}$$

and the corresponding boundary and matching conditions are

$$\tilde{u}_2 = \tilde{v}_2 = \tilde{w}_2 = 0 \quad \text{at} \quad \eta = 0 \quad \text{and} \quad \tilde{v}_2, \tilde{w}_2 \to 0 \quad \text{as} \quad \eta \to \infty. \tag{29}$$

We find that

$$\tilde{v}_2 \equiv 0. \tag{30}$$

Introducing the similarity variable $\zeta$, it is possible to express $\tilde{u}_2$ and $\tilde{w}_2$ in the following manner:

$$\tilde{u}_2 = (\dot{Q}/Q^2)(2s)^{\frac{1}{2}}[\tfrac{3}{2}f(\zeta) - \tfrac{1}{2}\zeta f'(\zeta)], \quad \tilde{w}_2 = (\dot{Q}/Q^2) s f'(\zeta), \tag{31}$$

where $f$ satisfies the equation

$$f''' + f_0 f'' - 2f_0' f' + 3f_0'' f = 2[f_0' + \tfrac{1}{2}\zeta f_0'' - 1], \tag{32}$$

with the boundary conditions

$$f(0) = f'(0) = f'(\infty) = 0,$$

whose numerical solution can be obtained in a straightforward manner.

The first-order boundary-layer solution can now be written in the form

$$w = Q[f_0'(\zeta) + \delta \cos\alpha \{f_0'(\zeta) + f_1'(\zeta) + s^2 f_2'(\zeta)\} + \epsilon(\dot{Q}/Q^2) s f'(\zeta)], \tag{33a}$$

where the first term is the quasi-steady Blasius profile for a straight tube, the middle term represents the curvature effect and the last term is due to the entrance velocity fluctuations. Similarly,

$$v = Q(\delta \sin\alpha \, s g'(\zeta)], \tag{33b}$$

$$u = \frac{\beta Q}{(2s)^{\frac{1}{2}}}[f_0(\zeta) - \zeta f_0'(\zeta) + \delta \cos\alpha\{f_1(\zeta) - \zeta f_1'(\zeta) + s^2(2g(\zeta) + 5f_2(\zeta) - \zeta f_2'(\zeta))\} + \epsilon(\dot{Q}/Q^2) s\{3f(\zeta) - \zeta f'(\zeta)\}], \tag{33c}$$

which include both the curvature and the entrance-velocity-fluctuation effects on the fluid motion near the pipe wall.

The curvature effect [see, for example, (33$a$)] is a small quantity of first order initially, but becomes larger as the flow develops further downstream. In fact, the above solution will no longer be valid for $s = O(\delta^{-\frac{1}{2}})$, as in the case of the steady-state analysis (Singh 1974).

Although the instantaneous Reynolds number varies in this study from small values to higher ones ($\sim 10^3$), it is the Reynolds number with respect to the mean speed which is important for the boundary-layer analysis and its value for the flow in the ascending aorta is quite large ($\sim 10^3$). However, it is the entrance-velocity fluctuation which has the most important bearing on our analysis, because the perturbation series (16) in powers of $\epsilon$ is no longer valid when

$$\epsilon s\dot{Q}/Q^2 = O(1), \tag{34}$$

which can be seen in the velocity fluctuation term in (33$a$) and which arises from the pressure gradient [see (15)] required to sustain the primary undisturbed flow. Although the frequency parameter $\epsilon$ is small ($\sim \frac{1}{10}$) in our study, the analysis may break down even close to the entrance at the instant when the instantaneous velocity $Q$ is very small and the acceleration $\dot{Q}$ is not correspondingly small, something which is likely to happen during the initial stages of the accelerating phase and concluding stages of the deceleration phase of the systole and throughout the diastolic phase (see Pedley 1976). In such a situation the flow will be approximately represented by a diffusive balance between the unsteady inertia terms and the viscous terms. Vorticity will continue to diffuse out into the fluid until convection once more becomes important. From the expression for the pressure in (11), it can be inferred that our analysis is valid so long as

$$\epsilon s|\dot{Q}|/Q^2 \lesssim \tfrac{1}{2} \tag{35}$$

(see also Pedley 1976).† In a subsequent study, it is proposed to present an analysis valid for the entire cycle as the blood is pumped from the left ventricle into the aorta.

The axial skin friction can now be written down from the above solution and is

$$\begin{aligned}\tau_{ws} &= -\left(\frac{\mu \overline{W}_0^3 Q^3 \rho}{2as}\right)^{\frac{1}{2}} \left[f_0''(0) + \delta\cos\alpha\{f_0''(0) + f_1''(0) + s^2 f_2''(0)\} + \epsilon s\frac{\dot{Q}}{Q^2} f''(0)\right] \\ &= -\left(\frac{\mu \overline{W}^3 Q^3 \rho}{2as}\right)^{\frac{1}{2}} \left[0{\cdot}4696 + \delta\cos\alpha(0{\cdot}2562 s^2 - 0{\cdot}9392) + \epsilon\frac{\dot{Q}}{Q^2}(1{\cdot}2s)\right].\end{aligned} \tag{36}$$

Here, the first term is the skin frinction for a straight tube with no velocity fluctuations at the entrance; their effects are represented by the last term. The middle term is the contribution from curvature. Both these effects increase as the flow develops further

† In fact, for the profile (3$a$), $Q = 1 + 0{\cdot}8\sin t$, taking $\epsilon = \frac{1}{10}$, we find that $\epsilon|\dot{Q}|/Q^2 \simeq 0{\cdot}2$ and so the boundary-layer analysis is valid throughout the cycle so long as $s \lesssim 0{\cdot}5/0{\cdot}2 = 2{\cdot}5$. On the other hand, for (3$b$),

$$Q = \begin{cases} (1-\cos\frac{8}{3}t)^3, & 0 \leqslant t \leqslant \frac{3}{4}\pi, \\ 0, & \frac{3}{4}\pi \leqslant t \leqslant 2\pi, \end{cases}$$

the boundary-layer analysis is not tenable even close to the entrance, from time $(0, \tau)$ and $(\frac{3}{4}\pi - \tau, 2\pi)$ where $\tau$ is given by $\epsilon|\dot{Q}(\tau)|/Q^2 = 0{\cdot}5$. In this case, initially there will be set up on the tube wall a diffusive (Rayleigh) layer. A quasi-steady boundary layer will thereafter be initiated at the entrance and will propagate downstream which will persist until after the time of peak velocity when a new diffusive layer takes over which persists until the end of the cycle ($t = 2\pi$) (see Pedley 1976).

downstream. In the middle term, the first expression is the effect of the secondary velocity and the second expression is the effect of reduced (increased) external flow and the longer (shorter) wall length traversed by the fluid at the outside (inside) of the bend. Since the effect of the secondary velocity on the skin friction is initially small, the fluid experiences less resistance in the outer part of the bend in comparison with that it would experience in a straight tube owing to the reduced external flow and the longer wall length; similarly it experiences increased resistance initially at the inside of the bend owing to the increased external flow and shorter wall length. The boundary layer of retarded fluid grows all round the tube, however the effect of the secondary flow, which increases with downstream distance, is to thin the boundary layer at the outside of the bend because retarded fluid is drawn off azimuthally, which results in reduced displacement and increased skin friction. On the other hand, the situation will be reversed for the inner side of the bend because the secondary flow brings in additional retarded fluid and thickens the boundary layer, which results in increased displacement and consequently a decrease in skin friction. The last term represents the entrance-velocity-fluctuation effect on the skin friction. It increases the skin friction during the accelerating phase through the accelerating pressure gradient and decreases it during the decelerating phase. Since the effect of velocity fluctuations on the skin friction increases as the flow develops further downstream, a situation arises in which negative shear stress exists which results in backflow – a phenomenon observed experimentally in arterial flows.

The azimuthal skin friction is given by

$$\tau_{w\alpha} = -(\rho\mu\overline{W}_0^3 Q^3/2as)^{\frac{1}{2}}\,\delta\sin\alpha\, sg''(0), \quad \text{where} \quad g''(0) = 1{\cdot}536. \tag{37}$$

There is no negative azimuthal shear stress because there is no adverse azimuthal pressure gradient in the primary flow. Accordingly, there will be no flow reversal so far as the azimuthal component of the velocity is concerned. The azimuthal wall stress increases as the fluid flows further downstream.

### *Flow due to displacement*

A careful examination of (33*c*) reveals that, except for the entrance-velocity-fluctuation term, the displacement effect on the core velocity can be derived from Singh's (1974) steady-case analysis by means of a suitable transformation as was done in the case of the boundary-layer analysis and so is not repeated here. We now obtain the contribution of the velocity-fluctuation term to the core velocity due to the displacement effect of the boundary layer.

From (33*c*) we find that as $\zeta\to\infty$, the term corresponding to the entrance-velocity-fluctuation effect is

$$\frac{\beta\epsilon}{(2s)^{\frac{1}{2}}}\frac{\dot{Q}}{Q^{\frac{3}{2}}}s[3f(\zeta Q^{\frac{1}{2}}) - \zeta Q^{\frac{1}{2}}f'(\zeta Q^{\frac{1}{2}})] \to \beta\epsilon\frac{\dot{Q}}{Q^{\frac{3}{2}}}\left(\frac{s}{2}\right)^{\frac{1}{2}} \times 3\beta_5, \tag{38}$$

where

$$\beta_5 = \lim_{\zeta=\infty} f = 0{\cdot}726964. \tag{39}$$

This would induce $O(\beta\epsilon)$ terms in the core velocity. As in the steady case (Singh 1974), we assume the following expansions for the core velocity:

(i) $$u(r,\alpha,s,t,\beta,\delta,\epsilon) = \beta[Q^{\frac{1}{2}}u^{(s)} + \epsilon\dot{Q}Q^{-\frac{3}{2}}U(r,\alpha,s) + \ldots], \tag{40a}$$

(ii) $v(r,\alpha,s,t,\beta,\delta,\epsilon) = \beta[Q^{\frac{1}{2}}v^{(s)} + \epsilon\dot{Q}Q^{-\frac{3}{2}}V(r,\alpha,s) + \ldots]$, (40*b*)

(iii) $w(r,\alpha,s,t,\beta,\delta,\epsilon) = Q/R(r,\alpha) + \beta[Q^{\frac{1}{2}}w^{(s)} + \epsilon\dot{Q}Q^{-\frac{3}{2}}W(r,\alpha,s) + \ldots]$, (40*c*)

(iv) $p(r,\alpha,s,t,\beta,\delta,\epsilon) = -\frac{1}{2}Q^2/R^2(r,\alpha) - \epsilon s\dot{Q} + \beta[Q^{\frac{3}{2}}p^{(s)} + \epsilon\dot{Q}Q^{-\frac{1}{2}}P(r,\alpha,s) + \ldots]$, (40*d*)

where $p^{(s)}$, $w^{(s)}$, $v^{(s)}$ and $u^{(s)}$ are given by (see Singh 1974)

$$p^{(s)} = \frac{1}{2\pi^{\frac{1}{2}}}\int_0^\infty \frac{\sin\sigma s\,d\sigma}{I_1(\sigma)}\left[-2\beta_1\sigma^{-\frac{1}{2}}I_0(\sigma r) + \delta\cos\alpha\left\{\frac{-I_1(\sigma r)\mathscr{J}(\sigma)}{I_0(\sigma)+I_2(\sigma)} + \beta_1(\sigma^{\frac{1}{2}}r^2I_1(\sigma r) + 5\sigma^{-\frac{1}{2}}rI_0(\sigma r))\right\}\right], \quad (41a)$$

$$w^{(s)} = \frac{1}{2\pi^{\frac{1}{2}}}\int_0^\infty \frac{\sin\sigma s\,d\sigma}{I_1(\sigma)}\left[2\beta_1\sigma^{-\frac{1}{2}}I_0(\sigma r) + \delta\cos\alpha\left\{\frac{I_1(\sigma r)\mathscr{J}(\sigma)}{I_0(\sigma)+I_2(\sigma)} - \beta_1(\sigma^{\frac{1}{2}}r^2I_1(\sigma r) + 3\sigma^{-\frac{1}{2}}rI_0(\sigma r))\right\}\right], \quad (41b)$$

$$v^{(s)} = \frac{\delta\sin\alpha}{2\pi^{\frac{1}{2}}r}\int_0^\infty \frac{\cos\sigma s\,d\sigma}{\sigma I_1(\sigma)}\left[\frac{I_1(\sigma r)\mathscr{J}(\sigma)}{I_0(\sigma)+I_2(\sigma)} - \beta_1\{\sigma^{\frac{1}{2}}r^2I_1(\sigma r) + \sigma^{-\frac{1}{2}}rI_0(\sigma r)\}\right], \quad (41c)$$

$$u^{(s)} = \frac{1}{4\pi^{\frac{1}{2}}}\int_0^\infty \frac{-\cos\sigma s\,d\sigma}{I_1(\sigma)}\left[4\beta_1\sigma^{\frac{1}{2}}I_1(\sigma r) + \delta\cos\alpha\left\{-2\beta_1(2\sigma^{\frac{1}{2}}rI_1(\sigma r) + \sigma^{-\frac{1}{2}}I_0(\sigma r) + \sigma^{\frac{1}{2}}r^2I_0(\sigma r)) + \frac{I_0(\sigma r)+I_2(\sigma r)}{I_0(\sigma)+I_2(\sigma)}\sigma\mathscr{J}(\sigma)\right\}\right], \quad (41d)$$

where

$$\mathscr{J}(\sigma) = 3\sigma^{-\frac{1}{2}}(2\beta_2+5\beta_4)I_1(\sigma) + 2\sigma^{-\frac{3}{2}}\beta_1 I_0(\sigma) + 4\sigma^{-\frac{1}{2}}(\beta_1+\beta_3)I_1(\sigma) + 2\beta_1\sigma^{\frac{1}{2}}I_0(\sigma).$$

Substituting (40) in (5)–(8), collecting the $O(\beta\epsilon)$ terms and using the matching condition from (38) gives

$$U = (\tfrac{1}{2}s)^{\frac{1}{2}}3\beta_5 \quad \text{at} \quad r = 1 \quad (42)$$

and the entry condition

$$U = V = W = 0 \quad \text{at} \quad s = 0. \quad (43)$$

We find that

$$V \equiv 0 \quad (44)$$

and $U$, $W$ and $P$ satisfy the following equations:

$$U_r + U/r + W_s = 0, \quad (45a)$$

$$\tfrac{1}{2}u_{10} + U_s = -P_r, \quad (45b)$$

$$\tfrac{1}{2}w_{10} + W_s = -P_s, \quad (45c)$$

where $u_{10}$ and $w_{10}$ are obtained from $u^{(s)}$ and $w^{(s)}$ by putting $\delta = 0$ and satisfying the continuity equation (45*a*) (see Singh 1974).

Elimination of $U$ and $W$ from (47) leads to

$$P_{rr} + r^{-1}P_r + P_{ss} = 0. \quad (46)$$

The matching condition (42) yields

$$P_r = (\beta_1 - 3\beta_5)/2(2s)^{\frac{1}{2}} \quad \text{at} \quad r = 1$$
$$= -\beta_6/2(2s)^{\frac{1}{2}}, \quad (47)$$

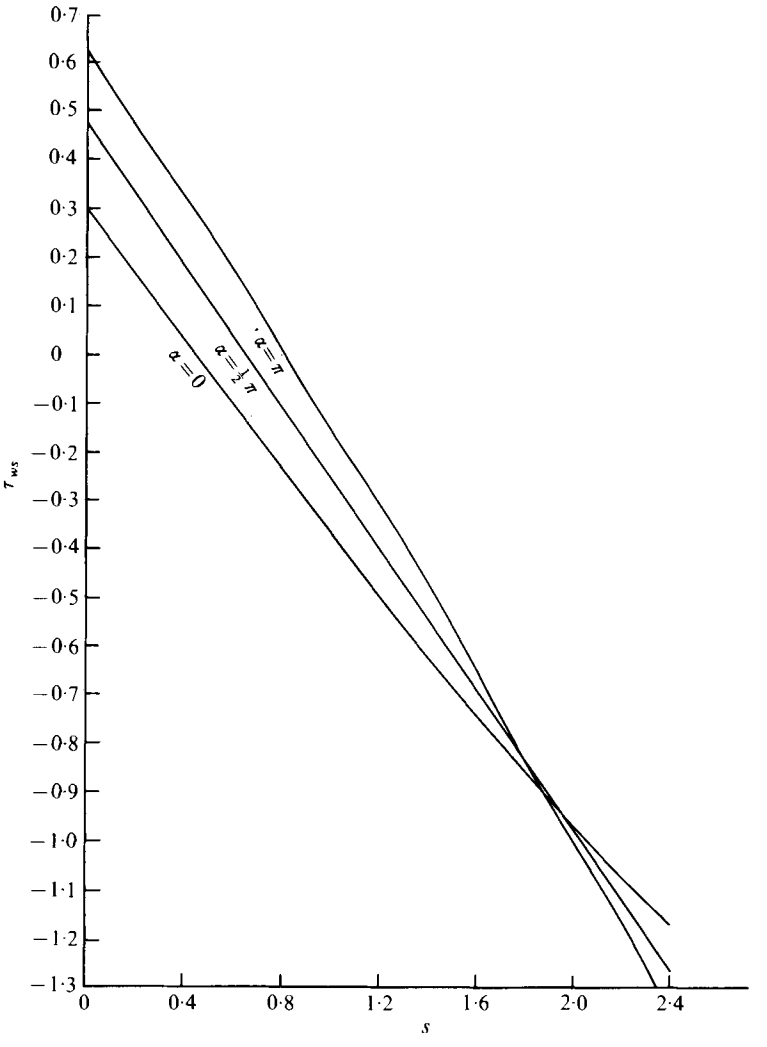


FIGURE 3. Axial skin friction $\tau_{ws}$ *vs.* $s$ for different values of $\alpha$ for the profile (3*a*). $t = \frac{5}{4}\pi$, $\epsilon = 0{\cdot}2$.

where

$$\beta_1 = 1{\cdot}21678$$

and hence

$$\beta_6 = 0{\cdot}9641. \tag{48}$$

The entry condition (43) implies

$$P = 0 \quad \text{at} \quad s = 0. \tag{49}$$

Equation (46) with boundary conditions (47) and (49) can be solved by applying Fourier sine transformation. We accordingly obtain the following solution:

$$P = -\frac{\beta_6}{2\pi^{\frac{1}{2}}} \int_0^\infty \frac{\sigma^{-\frac{3}{2}} I_0(\sigma r) \sin \sigma s \, d\sigma}{I_1(\sigma)}, \tag{50a}$$

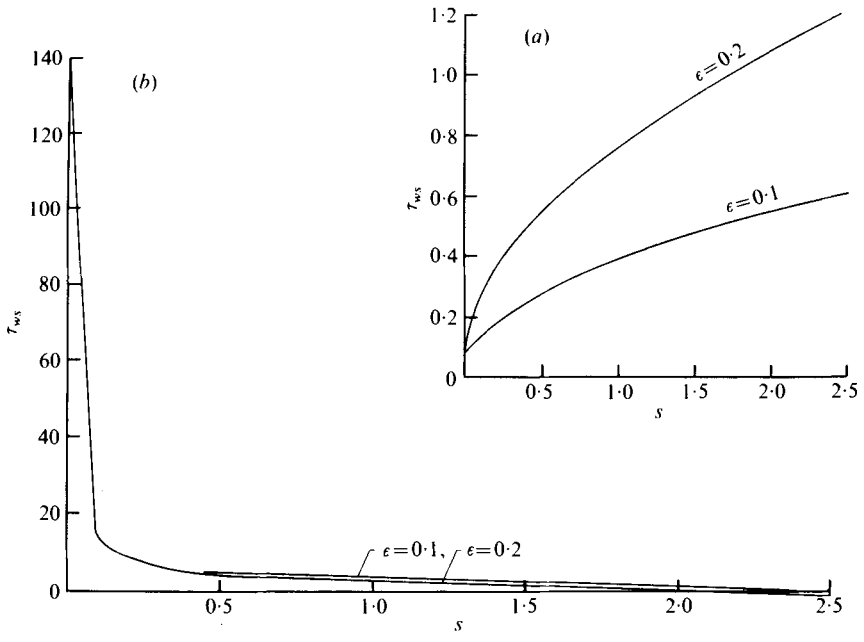


FIGURE 4. Axial skin friction $\tau_{ws}$ *vs.* $s$ for $\epsilon = 0{\cdot}1$ and $0{\cdot}2$ at the inner bend at (*a*) $t = 0{\cdot}3$ and (*b*) $t = 1{\cdot}5$ for the profile (3*b*). $\alpha = \pi$, $\delta = 0{\cdot}167$.

$$W = \frac{1}{2\pi^{\frac{1}{2}}}\int_0^\infty \frac{\sigma^{-\frac{3}{2}}I_0(\sigma r)}{I_1(\sigma)}\left[\beta_6 \sin\sigma s + \beta_1(\cos\sigma s - 1)\right]d\sigma, \tag{50b}$$

$$U = \frac{1}{2\pi^{\frac{1}{2}}}\int_0^\infty \frac{\sigma^{-\frac{3}{2}}I_1(\sigma r)}{I_1(\sigma)}\left[\beta_1 \sin\sigma s - \beta_6 \cos\sigma s\right]d\sigma. \tag{50c}$$

## 4. Results and discussion

### *Boundary layer*

We are now in a position to discuss the effects of various parameters on the flow fields.

### *Wall shear stress*

Figure 3 shows the relation between $\tau_{ws}$ and $s$ at $t = \frac{5}{4}\pi$ (decelerating phase of the systole) with $\epsilon = 0{\cdot}2$ and $Q = 1 + 0{\cdot}8\sin t$. Since, initially, the secondary-velocity and entrance-velocity-fluctuation effects are small, the diagram shows higher wall shear at the inner bend compared with that at the outer bend near the entrance owing to the larger external flow and the shorter wall length traversed by the fluid at the inside of the bend. Accordingly, as the flow develops, negative wall shear occurs first at the outer bend (at $t = \frac{5}{4}\pi$) owing to the adverse pressure gradient (proportional to $\dot{Q}$), but soon the secondary velocity grows, resulting in the reversal of the wall shear distribution in that, further downstream, larger wall shear occurs at the outer bend in comparison with the inner bend as shown in figure 3. The wall shear decreases as $s$ increases because the quasi-steady boundary layer becomes thicker as the flow develops.

Figure 4 represents the effect of the frequency parameter $\epsilon$ on $\tau_{ws}$ for the profile (3*b*). At time $t = 0{\cdot}3$, the pressure gradient term $\dot{Q}/Q^2$ is comparatively large and so

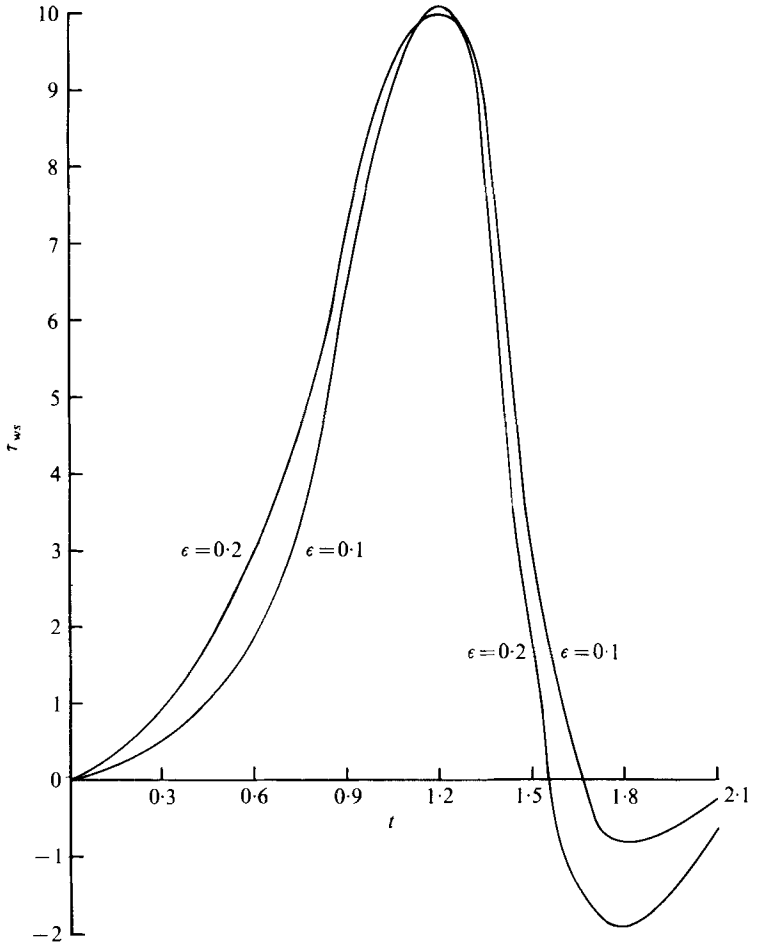


FIGURE 5. Axial skin friction $\tau_{ws}$ *vs.* $t$ at the outer bend for $\epsilon = 0{\cdot}1$ and 0·2 for the profile (3*b*). $s = 1{\cdot}5$, $\alpha = 0$, $\delta = 0{\cdot}167$.

an increase in $\epsilon$ significantly increases the wall shear stress in figure 4 (*a*). On the other hand, in figure 4 (*b*), $\dot{Q}/Q^2$ is comparatively small at $t = 1{\cdot}5$ and so the value of wall shear stress is not significantly altered by changing the value of $\epsilon$ from 0·1 to 0·2.

Further, in figure 4 (*a*), the wall stress increases with $s$ in contrast to figure 4 (*b*) in which it decreases as $s$ increases owing to the boundary layer becoming thicker. This peculiar behaviour in figure 4 (*a*) is due to the fact that the pressure gradient term in the wall stress is the dominating term which increases as $s$ increases (refer to (34) and the corresponding discussion).

Similar influence of the frequency parameter on the wall stress is reflected by figure 5, which shows $\tau_{ws}$ *vs.* $t$ at $s = 1{\cdot}5$ for $\epsilon = 0{\cdot}1$ and 0·2 for the entrance profile $Q$ given by (3*b*). It shows that the shear stress reverses its sign although the outer flow does not. This is because the slower moving fluid near the wall responds more rapidly to the applied adverse pressure gradient (associated with the rapid deceleration of the core flow as the aortic valve closes) than does the free stream. The same reason applies to the slight phase lead of the peak in $\tau_{ws}$ over that of the free-stream

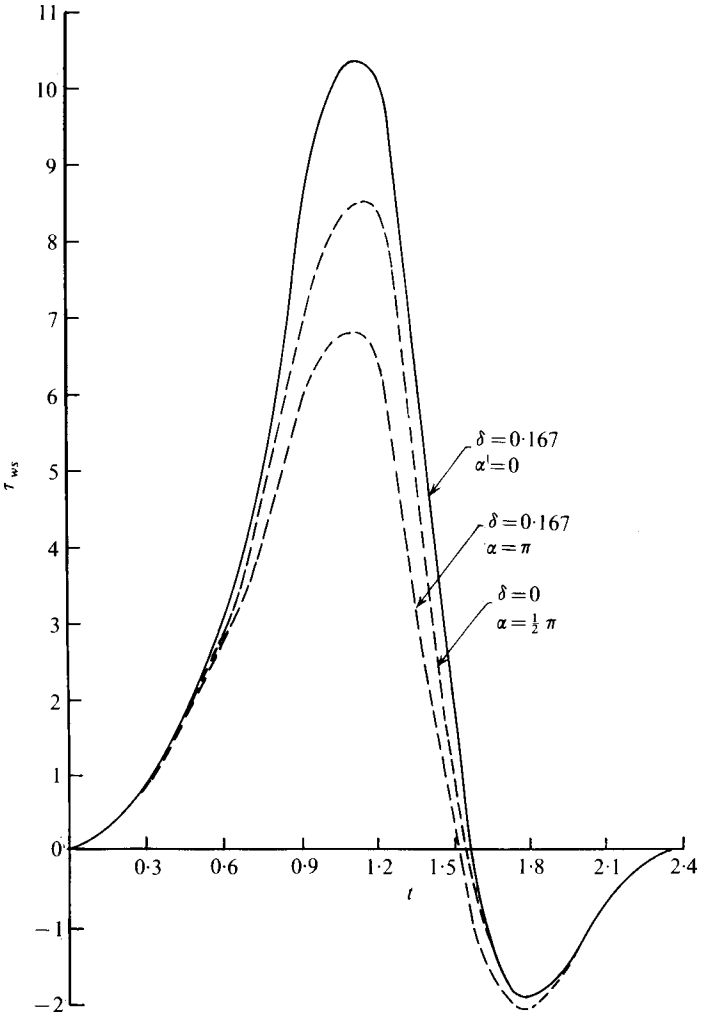


FIGURE 6. Axial skin friction $\tau_{ws}$ *vs.* $t$ at the inner and outer bends (and also for the straight tube) for the profile (3*b*). $s = 1{\cdot}5$, $\epsilon = 0{\cdot}2$.

peak velocity reflected by the graphs in figure 6 which represent the variation of $\tau_{ws}$ with $t$ at the inner and outer bends (and also for the straight tube) for the entrance profile given by (3*b*) at $s = 1{\cdot}5$ when the secondary flow as well as the entrance-velocity fluctuation have significant effects on the wall stress. The larger wall stress at the outer bend compared with its value at the inner bend has already been accounted for in the discussions of the graphs in figure 3. The magnitude of the difference in wall shear at the outer and inner bends depends on (i) the effect of the secondary flow and (ii) the magnitude of the entry flow which is at the peak near $t = \frac{3}{8}\pi$ in figure 6 and near $t = \frac{1}{2}\pi$ in figure 7 (*a*).

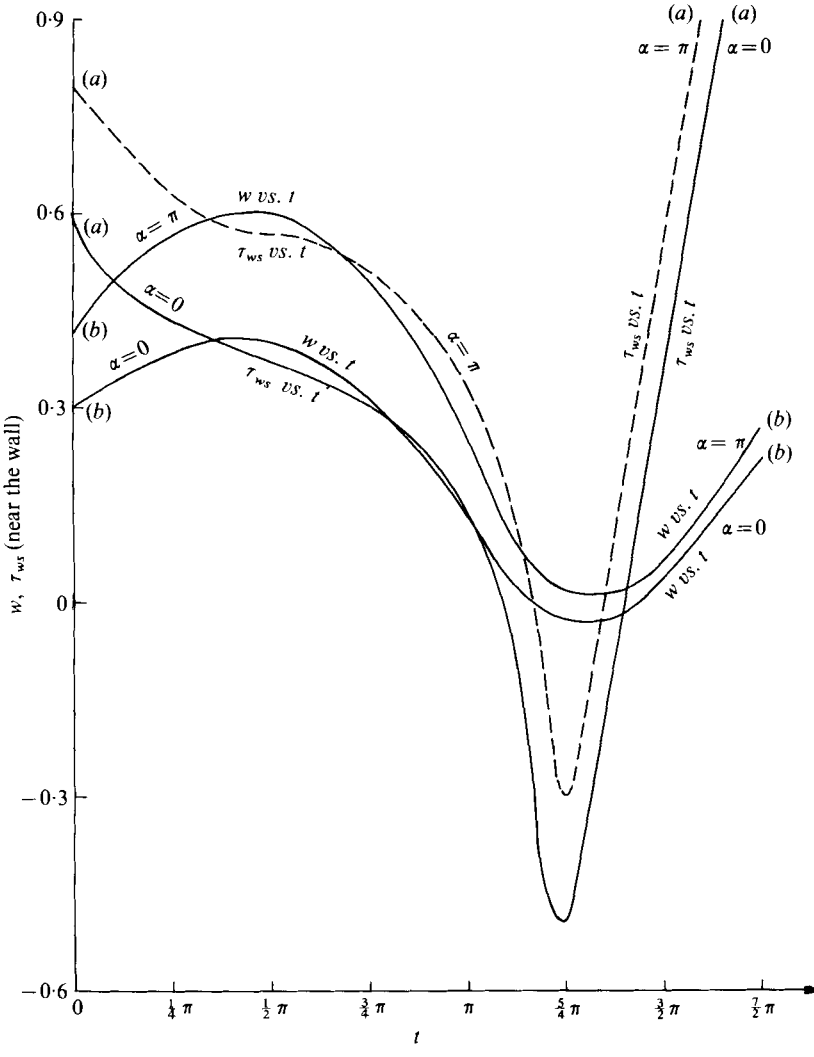


FIGURE 7. Variation of streamwise velocity near the wall ($\zeta = 0{\cdot}2$) and the axial skin friction with time at the inner and outer bends for the profile (3*a*). $s = 1{\cdot}2$, $\epsilon = 0{\cdot}2$.

*Streamwise velocity*

$$w = Q\left[f_0'(\zeta) + \delta\cos\alpha\{f_0'(\zeta) + f_1'(\zeta) + s^2 f_2'(\zeta)\} + \epsilon\frac{\dot{Q}}{Q^2}sf'(\zeta)\right].$$

Here, the first term on the right-hand side is the quasi-steady Blasius boundary-layer term and the second term represents the curvature effect; the first two terms inside the curly brackets represent the variation of the Blasius boundary layer with $\alpha$ owing, respectively, to (i) dependence on $\alpha$ of the flow velocity just outside the boundary layer and (ii) dependence on $\alpha$ of the distance traversed along the curved wall for given $s$, and the third term represents the development of the secondary flow. It shows how the curvature effect, which is initially of second order, grows as the fluid flows further downstream. The last term is the effect of entrance-velocity fluctuations, which increases as the flow develops further downstream.

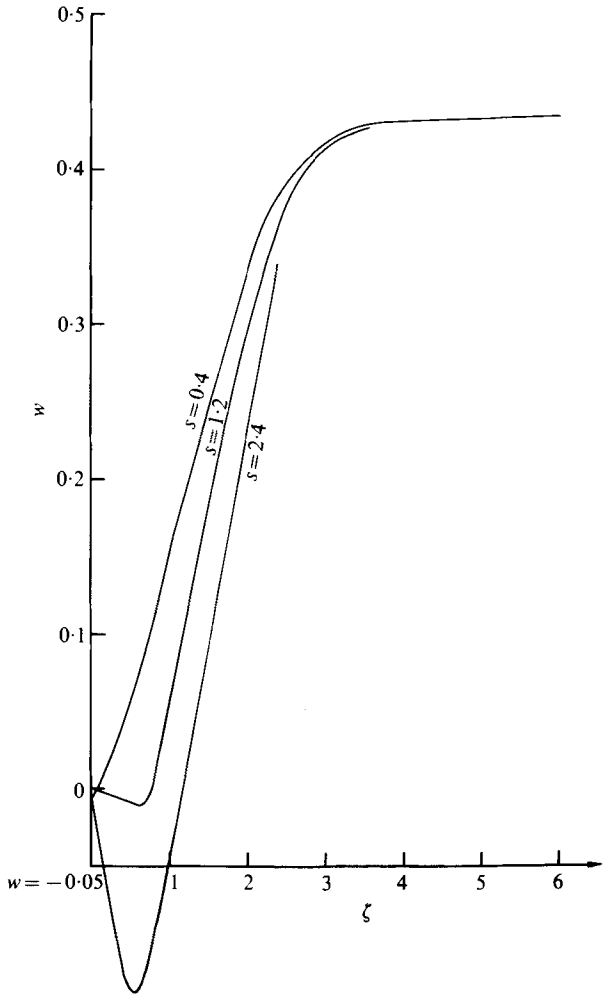


FIGURE 8. Streamwise velocity $w$ *vs.* $\zeta$ for different values of $s$ for profile (3*a*) (straight-tube case). $t = \frac{5}{4}\pi$, $\alpha = \frac{1}{2}\pi$.

Figure 7(*b*) shows how the streamwise velocity changes with $t$ for $Q = 1 + 0{\cdot}8\sin t$ at $s = 1{\cdot}2$ when the secondary-velocity and the entrance-velocity-fluctuation effects no longer remain small. The graphs show that the streamwise velocity is larger near the inner bend compared with its value near the outer bend. This implies that the effects of the external flow and of geometrical factors still dominate the growing effect of the secondary flow which draws off azimuthally the slower moving fluid particles in the boundary layer from the outside of the bend towards the inside and takes faster moving fluid particles from the inside to the outside of the bend. The difference in magnitude of their values (i.e. of $w$) is maximum when the entry velocity has reached its peak (i.e. near $t = \frac{1}{2}\pi$). Further, the graphs indicate that although there is no flow reversal of the free stream, backflow of the fluid particles near the outer bend in the boundary layer takes place during a part of the decelerating phase, whereas near the inner bend no flow reversal takes place at this stage. This can be accounted for in the same way as we discussed the negative wall shear stress in the

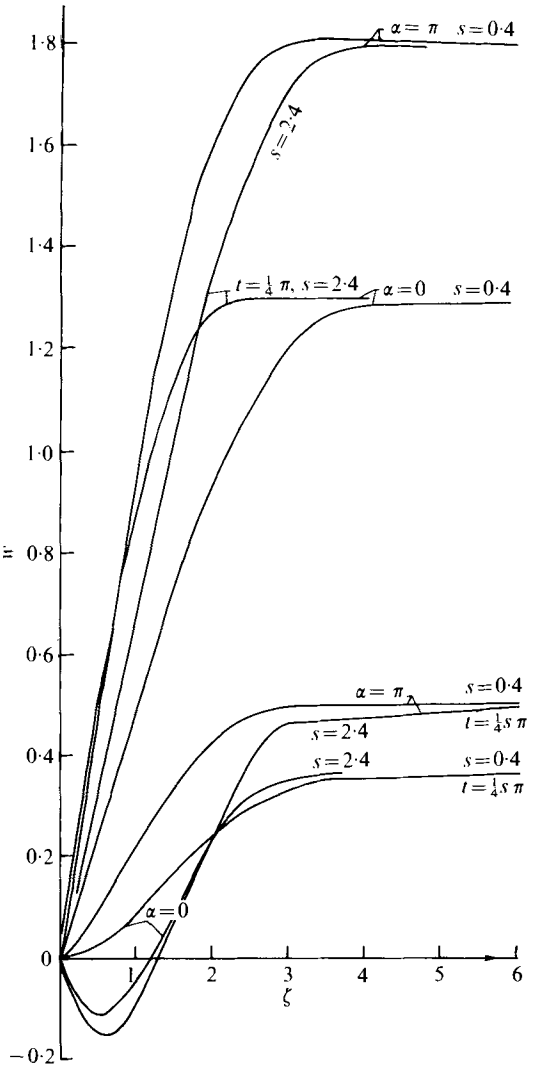


FIGURE 9. Streamwise velocity $w$ *vs.* $\zeta$ for the profile (3*a*) for different values of $s$ and $t$.

preceding paragraphs. The slower moving fluid near the outer bend responds more readily to the applied adverse pressure gradient than does the faster moving fluid near the inner bend. As the effects of secondary flow and entrance-velocity fluctuation increase further downstream, flow reversal (during a part of the decelerating phase) near the inner bend can also be expected. The slight phase lead of the streamwise velocity in the boundary layer over that of the free-stream velocity can be similarly accounted for.

Figure 8 represents the variation of $w$ in the boundary layer (for the straight-tube case) at $t = \frac{5}{4}\pi$ (which is the time for $Q = 1 + 0{\cdot}8 \sin t$ when the decelerating phase has fairly strong influence on the flow) for various values of $s$. It shows how the backflow develops near the wall as the effect of adverse pressure gradient increases further downstream.

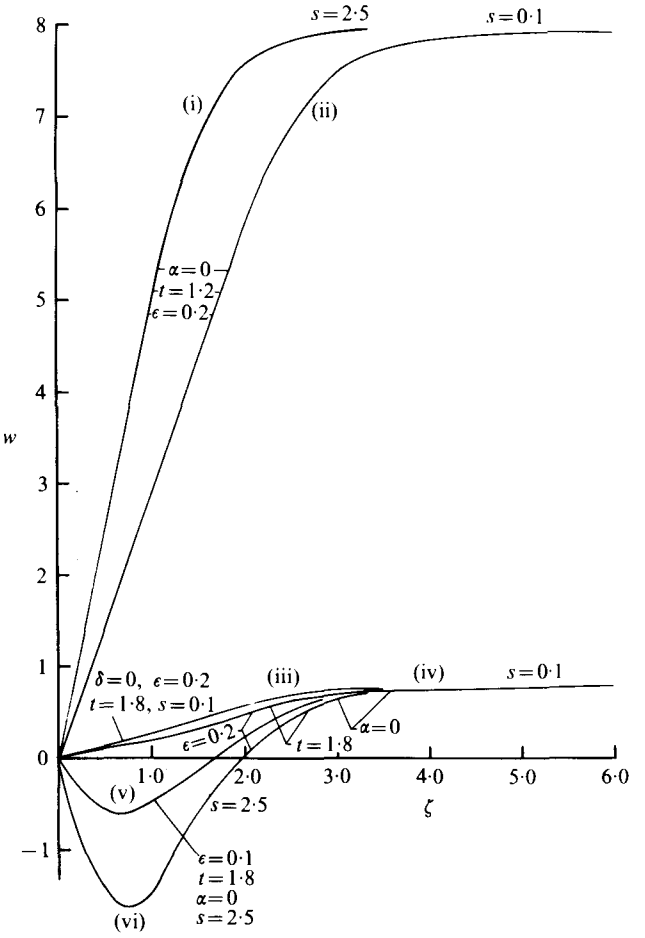


FIGURE 10. Streamwise velocity $w$ *vs.* $\zeta$ for the profile (3*b*).

Figure 9 represents the variation of streamwise velocity in the boundary layer for $Q = 1 + 0{\cdot}8 \sin t$ near the inner and outer bends at two different phases of the cycle ($t = \frac{1}{4}\pi$ and $\frac{5}{4}\pi$) for $s = 0{\cdot}4$ and $2{\cdot}4$. Initially (see the graphs at $s = 0{\cdot}4$), the profiles are steeper near the inner bend in comparison to the outer bend owing to (i) the influence of the external flow and (ii) the shorter wall length described by the fluid particles near the inner bend. As the flow develops, the effect of the secondary flow increases, which draws off the retarded fluid particles azimuthally at the outer bend and induces a cross-flow from the inner bend to the outer bend which results in the thinning of the boundary layer at the outer bend and its thickening at the inner bend. This is reflected by the profiles: near the inner bend, the graph is steeper at $s = 0{\cdot}4$ in comparison with $s = 2{\cdot}4$ owing to thickening of the boundary layer further downstream. On the other hand, the situation is reversed near the outer bend (during the accelerating phase) owing to the thinning of the boundary layer. As pointed out, initially the curves are steeper near the inner bend, the situation reverses during the accelerating phase as the flow develops further downstream owing to the increasing effect of the secondary flow in that the curve is steeper at the outer bend (compare the graphs

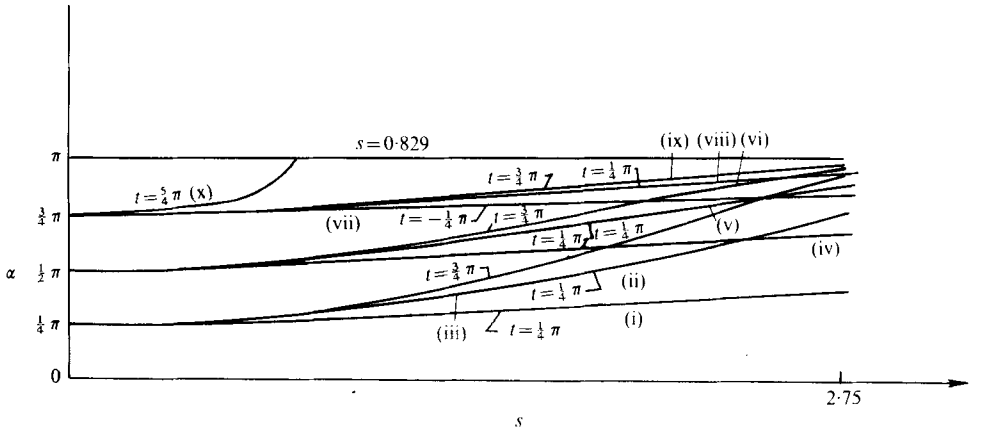


FIGURE 11. Limiting streamlines at various instants of cycle for the profile (3*a*).

at $s = 2{\cdot}4$ for the accelerating phase). A similar situation is reflected by the graphs for the decelerating phase except that the backflow occurs near the wall as the flow develops owing to the increasing effect of the adverse pressure gradient. Notice that the slower moving fluid near the inner bend responds more readily to the adverse pressure gradient than the faster moving fluid near the outer bend (compare the graphs at $s = 2{\cdot}4$ and $t = \frac{5}{4}\pi$).

A similar situation is reflected by the graphs of $w$ *vs.* $\zeta$ (see figure 10) for the profile (3*b*). At $t = 1{\cdot}2$ (see graphs (i) and (ii)), when the entrance velocity is almost at its peak, the graph is steeper at $s = 2{\cdot}5$ than at $s = 0{\cdot}1$ near the outer bend owing to the effect of secondary velocity. At such an instant the entrance-velocity-fluctuation effect would be very small and so we shall not expect much difference in the graphs for the values of the frequency parameter $\epsilon = 0{\cdot}1$ and $0{\cdot}2$ (the graph for $\epsilon = 0{\cdot}1$ is not shown). During the decelerating phase ($t = 1{\cdot}8$ when the effect of the velocity fluctuation would be almost maximum), the velocity does not change much with $\alpha$ (see graphs (iii) and (iv)) near the entrance because the effect of secondary flow is comparatively smaller at the initial stages of flow development and the external flow is also small at this instant. Graphs (v) and (vi) illustrate the influence of the adverse pressure gradient on the flow, which accounts for the backflow near the wall. For such a situation, clearly, the value of the frequency parameter would play a significant role as can be seen by comparing (v) and (vi).

### *Limiting streamlines*

The equation for the limiting streamlines at the wall can be written as

$$d\alpha/ds = \lim_{r\to 1} v/w = \lim_{r\to 1} v_r/w_r = \tau_{w\alpha}/\tau_{ws}.$$

Therefore

$$d\alpha/ds = \delta \sin\alpha\, sg''(0)/[f_0''(0) + \delta\cos\alpha\,[f_0''(0) + f_1''(0) + s^2 f_2''(0)] + \epsilon(\dot{Q}/Q^2)\, sf''(0)].$$

These streamlines are plotted in figure 11. Along the inner and outer bends, there is no azimuthal pull and since the azimuthal velocity is also zero, the streamlines are straight there as in the steady case (Singh 1974). At any other point on the wall, the

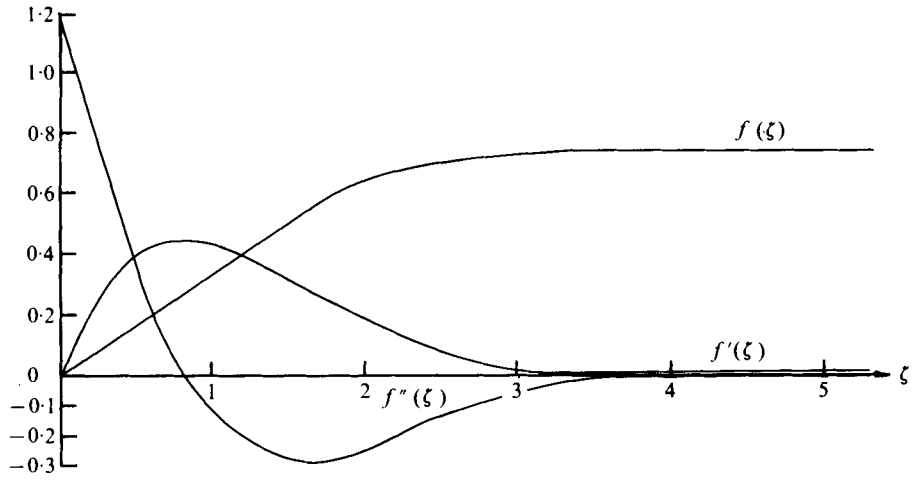


FIGURE 12. Graph of $f$, $f'$ and $f''$ *vs.* $\zeta$ (effect of entrance velocity fluctuations in the boundary layer.)

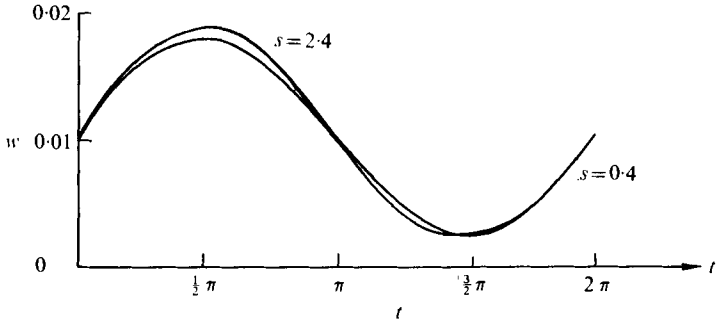


FIGURE 13. Streamwise velocity $w$ *vs.* $t$ at the centre-line for $s = 0{\cdot}4$ and $2{\cdot}4$ for the profile (3*a*).

streamlines tend to move towards the inner bend because of the azimuthal pull in that direction. The rapid variation of these limiting streamlines at various instants of the cycle is depicted in figure 11; it depends, of course, on the relative magnitude of $\tau_{ws}$ and $\tau_{w\alpha}$. As the external flow decelerates, the streamwise wall shear tends to decrease until it vanishes as the flow develops with the result that the limiting streamlines would converge at this point (provided it is at the inner or outer bend where $\tau_{w\alpha} = 0$), as is shown in the case of streamline $x$ at the time $t = \frac{5}{4}\pi$.

Figure 12 shows how the function $f$ and its derivatives vary with $\zeta$. These functions essentially represent the effect of the entrance-velocity fluctuation on the flow fields in the boundary layer. The function $f'$, which represents this effect on $w$, sharply increases near the wall and then decays to zero. Similarly $f''$ essentially represents the vorticity generated in the boundary layer owing to the entrance-velocity fluctuation and it is maximum at the wall and then falls rapidly to negative values and thereafter decays as the edge of the boundary layer is approached.

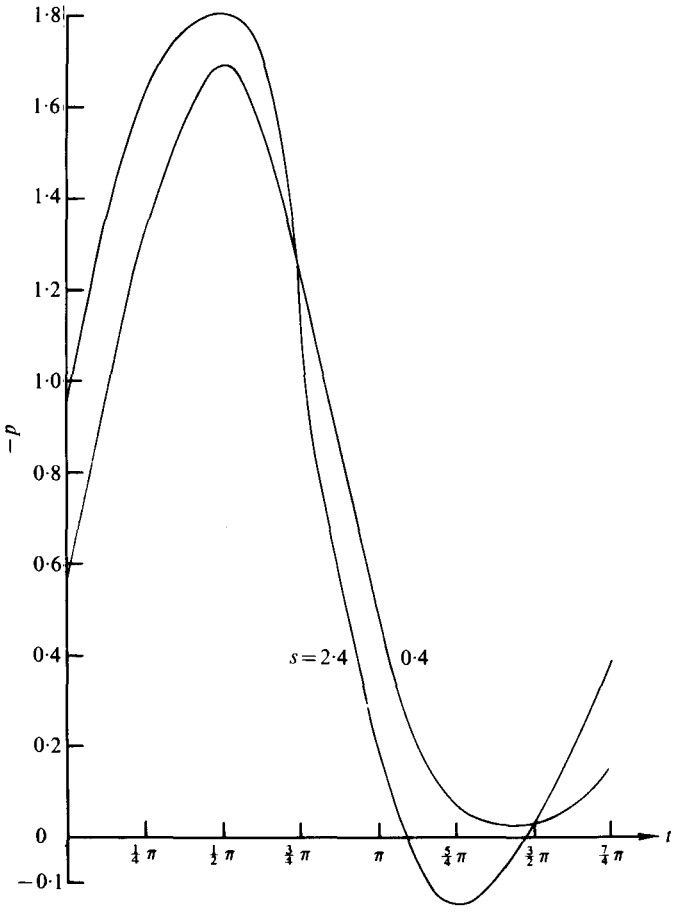


FIGURE 14. Pressure *vs.* time at the centre-line for $s = 0{\cdot}4$ and 2·4 for the profile (3*a*).

### *Inviscid core*

Figure 13 shows the displacement effect of the boundary layer on $w$ in the core. It is seen that this effect is not significant. The maximum change in $w$ due to the displacement effect of the boundary layer is at $t = \frac{1}{2}\pi$, the instant when the external flow velocity is maximum. This is understandable because if we assume (see Pedley 1976) that the fluid everywhere in the tube comes to rest by the end of the cycle, so that each beat can be treated as an isolated event, with the velocity initially zero, it implies that the thickness of the boundary layer which develops at the tube wall during every beat will be of the order of $(\nu T)^{\frac{1}{2}}$, which (taking $\nu = 0{\cdot}038$ in cgs units and $T = \frac{6}{7}$ s) is approximately equal to 0·13 cm, about one-tenth of the vessel diameter. Thus, in view of the boundary layer remaining thin during each cycle, the displacement effect is not very significant.

As the boundary layer grows, figure 14 shows how the pressure drops with streamwise distance during the accelerating phase and how the adverse pressure gradient changes with $s$ during the decelerating phase. Again, the displacement effect is not expected to be significant as in the steady case (Singh 1974).

The study was initiated and to a considerable extent completed at Cambridge, where one of the authors (Singh) was visiting under the auspices of the Imperial College, Delhi Committee, London. The authors wish to express their thanks to Professor Lighthill (at whose suggestion this study has been taken up) for his continued interest in this work. Thanks are also due to Dr Pedley for useful discussions.

## REFERENCES

BELLHOUSE, B. J. & TALBOT, L. 1969 *J. Fluid Mech.* **35**, 721.

CARO, C. G., FITZ-GERALD, J. M. & SCHROTER, R. C. 1971 *Proc. Roy. Soc.* A **177**, 109.

CHANDRAN, K. B., SWANSON, W. M., GHISTA, D. N. & VAYO, H. W. 1974 *Ann. Biomed. Engng* **2**, 392.

HALL, P. & PARKER. K. 1976 *J. Fluid Mech.* **75**, 305.

LIGHTHILL, M. J. 1975 *Mathematical Biofluiddynamics*. Philadelphia: SIAM.

MCDONALD, D. A. 1952 *J. Physiol.* **118**, 328.

MCDONALD, D. A. 1960 *Blood Flow in Arteries*. Edward Arnold.

NEREM, R. M. & SEED, W. A. 1972 *Cardiovasc. Res.* **6**, 1.

NEREM, R. M., SEED, W. A. & WOOD, N. B. 1972 *J. Fluid Mech.* **52**, 137.

OLSON, D. E. 1971 Fluid mechanics relevant to respiratory flow within curved or elliptic tubes and bifurcating systems. Ph.D. thesis, Imperial College, London.

PATANKAR, S. V., PRATAP, V. S. & SPALDING, D. B. 1974 *J. Fluid Mech.* **62**, 539.

PEDLEY, T. J. 1976 *J. Fluid Mech.* **74**, 59.

SEED, W. A. & WOOD, N. B. 1971 *Cardiovasc. Res.* **5**, 319.

SINGH, M. P. 1974 *J. Fluid Mech.* **65**, 517.

WHITMORE, R. L. 1968 *Rheology of the Circulation*. Pergamon.

WOLSTRAHOLME, G. E. W. & KNIGHT, J. 1973 *CIBA Symp.* Amsterdam: Assoc. Sci. Publ.

YAO, L. S. & BERGER, S. A. 1975 *J. Fluid Mech.* **67**, 177.